Fuel 172 (2016) 248–252

Contents lists available at ScienceDirect

Fuel

journal homepage: www.elsevier.com/locate/fuel

Optimized rate expressions for soot oxidation by OH and O_2

Haiqing Guo, Paul M. Anderson, Peter B. Sunderland *

Department of Fire Protection Engineering, 3104 J.M. Patterson Building, University of Maryland, College Park, MD 20742, USA

ARTICLE INFO

Article history:
Received 3 October 2015
Received in revised form 2 January 2016
Accepted 7 January 2016
Available online 13 January 2016

Keywords:
Combustion
Fire
Flames
Particulates

ABSTRACT

The two principal soot oxidizers in flames are the hydroxyl radical (OH) and molecular oxygen (O_2). Many soot oxidation rate expressions exist for these oxidizers, but they have considerable disparity and have not been sufficiently validated. To address this, twelve published experimental studies in diffusion flames, premixed flames, thermogravimetric analyzers, and flow reactors are examined. These are all the known studies that measured all of the following quantities at discrete locations: soot oxidation rate, temperature, OH concentration (if nonzero), and O_2 concentration. This yielded 160 measured soot oxidation rates spanning seven orders of magnitude. Optimized soot oxidation rate expressions for OH and O_2 are developed here by maximizing the coefficient of determination between measured and modeled oxidation rates. Oxidation of soot by OH is found to have a negligible activation energy and a collision efficiency of 0.10. The activation energy for O_2 oxidation of soot is 195 kJ/mol, which is higher than previous models. The new expressions for OH and O_2 match the measurements with a regression coefficient of 0.98, compared to 0.79 for the most widely used models. The optimized models indicate that soot oxidation in flames by OH generally dominates over that by O_2.

1. Introduction

Soot can be destroyed in flames via oxidation by OH, O_2, O, CO_2, and H_2O [1–3] and by the reversal of soot formation reactions [4–6]. Among these, soot oxidation by OH and O_2 generally dominates soot destruction in flames [7–10] and has been the primary focus of both experimental [8–15] and numerical [4–6,16–19] studies. These oxidation reactions are generally considered to be:

$$C_{soot} + OH \rightarrow CO + \text{products}, \quad \text{and} \tag{1}$$

$$C_{soot} + O_2 \rightarrow 2CO + \text{products}. \tag{2}$$

There is considerable disparity and uncertainty in the existing soot oxidation rate models for OH and O_2. Furthermore, none of the models has been systematically compared to a broad set of measurements. Thus motivated, the objective of this study is to develop optimized soot oxidation rate expressions for OH and O_2 using a broad set of published measurements.

1.1. Existing models for soot oxidation by OH

Fenimore and Jones [20] were among the first to recognize the importance of OH as a soot oxidant in flames. They considered a two-stage premixed burner where soot-laden combustion gases from the first stage were mixed with air and burned in the second stage. They reported an OH collision efficiency of $\eta_{OH} = 0.1$.

Using a similar apparatus, Neoh and co-workers [9,10] found OH to be the principal soot oxidizer, with $\eta_{OH} = 0.13$. Corrections were made for soot oxidation by O_2 using Nagle and Strickland-Constable [21]. The model of Neoh and co-workers [9,10] remains the leading OH model, and has been widely adopted [4–6,19,22].

Soot oxidation by OH has also been observed in diffusion flames, at 0.1–8.0 bar [8,11–15]. Corrections for both growth by hydrocarbons and oxidation by O_2 generally were required, which resulted in the exclusion of many conditions with negative remaining oxidation. These studies reported η_{OH} to be between 0.01 and 0.4.

1.2. Existing models for soot oxidation by O_2

The most widely used model of soot oxidation by O_2 is that of Nagle and Strickland-Constable (NSC) [21]. They measured oxidation rates of heated carbon rods at temperatures of 1000–2000 °C and O_2 partial pressures, p_{O2}, of 0.1–0.6 bar. These conditions bear little resemblance to soot oxidation in flames. Furthermore, the NSC expression is often misused, as the original expression involved a typographical error and unusual units [23]. The NSC model has been incorporated into computational fluid dynamics (CFD) models [19,22].

* Corresponding author. Tel.: +1 (301) 405 3095; fax: +1 (301) 405 9383.
E-mail address: pbs@umd.edu (P.B. Sunderland).

http://dx.doi.org/10.1016/j.fuel.2016.01.030
0016-2361/

Another widely used model is that of Lee et al. [24], who observed soot oxidation in a propane–propylene–ethylene diffusion flame confined by a chimney. This model involves an activation energy of $E_A = 164.4$ kJ/mol and is valid for temperatures between 1300 and 1700 K and p_{O2} between 0.05 and 0.1 bar. This model was adopted by Leung et al. [17], albeit with a pre-exponential factor increased by a factor of eight.

A comparison of the O_2 soot oxidation rate predictions of NSC [21] and Lee et al. [24] is shown in Fig. 1 for typical flame conditions. The shaded regions identify the measurement ranges of these studies. The disagreement between models, up to a factor of 20 for these conditions, attests to the uncertainties in the leading soot oxidation models. Soot oxidation rate is generally predicted to increase with increasing p_{O2} or temperature. However, the NSC model [21] has a negative temperature coefficient at low p_{O2} and a decreased slope at high p_{O2}. Neither behavior has been validated for soot oxidation.

In CFD simulations, e.g., Refs. [25–27], a widely used soot oxidation model is that of Appel, Bockhorn, and Frenklach (ABF) [4–6]. ABF includes an Arrhenius form for soot oxidation by O_2 with $E_A = 31.3$ kJ/mol based on the low temperature oxidation of the phenyl radical (C_6H_5) in a shock tube [28]. The ABF soot oxidation rate by O_2 is [4]:

$$\dot{w}_{ox} = 2MW_C A_2 \exp(-E_{A,2}/R_uT)\chi_{C\cdot} p_{O_2}/(N_A R_u T), \quad (3)$$

where A_2 and $E_{A,2}$ are the pre-exponential factor and activation energy for Eq. (2); MW_C is molar mass of carbon; p_{O2} units are Pa; N_A is the Avogadro constant; R_u is the universal gas constant; and T is temperature. The active carbon site number density is

$$\chi_{C\cdot} = \frac{k_8[H]\chi_{C-H}}{k_{-8}[H_2] + k_9[H] + k_{10}[C_2H_2] + k_{11}[O_2]}, \quad (4)$$

where χ_{C-H} is the steady arm-chair site number density; the k are rate coefficients, numbered according to Ref. [4]; and brackets denote concentrations.

A comparison of the ABF [4] soot oxidation rates by O_2 with those of other models requires realistic conditions including temperature, soot surface area, and concentrations of H_2, H, C_2H_2, and O_2. The measurements of flame 1 of Xu et al. [8], fueled by C_2H_2, provide these. The soot oxidation rates by O_2 predicted for this flame by ABF, assuming $\chi_{C-H} = 2.3 \times 10^{19}$ sites/m^2 [4], are shown as a function of height above burner, z, in Fig. 2. Also shown are the predictions of two past models [21,24] and the present study (discussed below).

The models of Refs. [4,21,24] are not in good agreement for this flame. The ABF model predicts the lowest soot oxidation rates. This is most dramatic low in the flame where C_2H_2 mole fractions are as high as 0.17, reducing the active site density according to Eq. (4). Agreement with other models improves near $z = 50$ mm, where the C_2H_2 mole fraction has decreased to 0.01. The NSC [21] predictions are typically double those of Lee et al. [24] for this flame.

Although conditions in thermogravimetric analyzers (TGAs) and flow reactors are different from those in flames, they allow measurements at lower temperatures, longer residence times, and lower oxidation rates than can be achieved in conventional flames. Several studies have considered the low temperature oxidation of soot by O_2 in a TGA [29–35]. Chan et al. [29] did so at 770–1250 K, augmented with tests similar to those of Lee et al. [24] in the post-flame region, and reported $E_A = 143.5$ kJ/mol. Kalogirou and Samaras [30] observed the oxidation of diesel soot and synthetic soot in a TGA at 800–1000 K and reported $E_A = 161.2$ kJ/mol and a dependence on $p_{O2}^{0.75}$. Sharma et al. [31] observed the oxidation of diesel soot in a TGA at 800–900 K and reported $E_A = 155$ kJ/mol.

Higgins et al. [36] studied the oxidation of soot by O_2 at 1100–1400 K in a flow reactor. Soot mass was determined from soot particle mobility diameters. They reported $E_A = 164$ kJ/mol and a pre-exponential factor that varied with initial particle size by ±35%.

The activation energy for soot oxidation by O_2 is commonly compared with that obtained in coal combustion. Smith [3] reviewed the combustion of coke, char, graphite, and soot from various studies and obtained a mean activation energy of 179.1 kJ/mol. However, most coke or char particles are several orders of magnitude larger than soot primary particles. Soot primary particles, with typical diameters of 30 nm, are small enough that the diffusion of oxidants to the surface is fast and the oxidation process is kinetically controlled [9].

2. Past soot oxidation measurements

The open literature was searched for sufficiently detailed measurements of soot oxidation rates. Only conditions that reported all of these properties for mature soot were admitted: soot

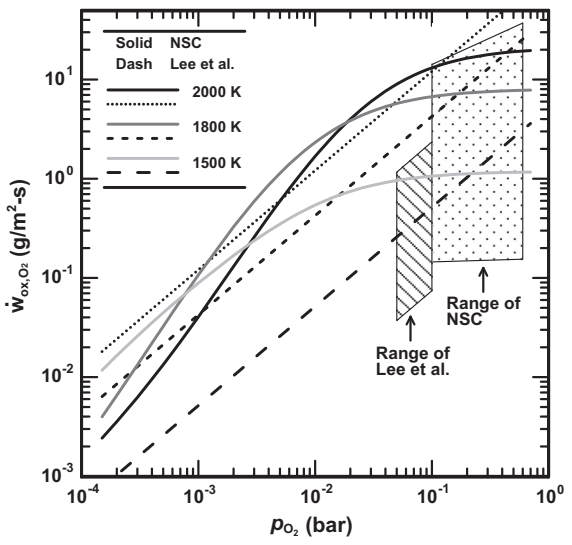

Fig. 1. Predictions of NSC [21], and Lee et al. [24] of soot oxidation rates by O_2 at various conditions. The shaded regions show the measurement ranges.

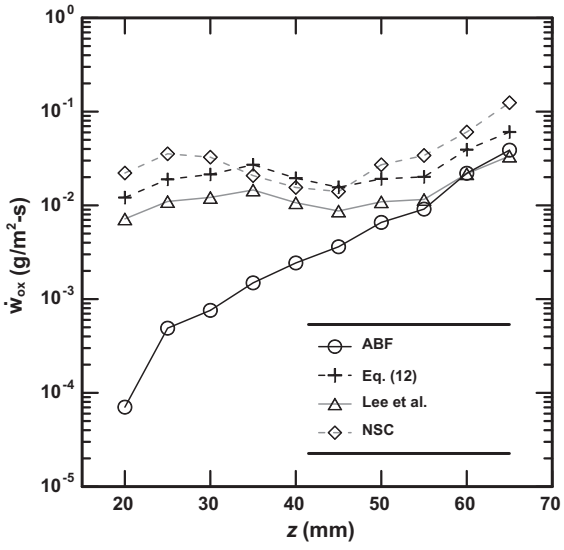

Fig. 2. Predicted soot oxidation rates by O_2 for flame 1 of Ref. [8] using the soot oxidation models of: ABF [4], see Eq. (3); Lee et al. [24]; NSC [21]; and the present model, see Eq. (12).

oxidation rate, temperature, OH concentration (if nonzero), and O_2 concentration. Studies that determined soot mass from transmission electron microscopy (TEM) were excluded for their high uncertainties. In most cases oxidation rates were provided in, or readily converted to, units of soot mass loss rate per soot surface area. The only exceptions were Refs. [30,31], as discussed below. Table 1 summarizes the 160 conditions from 12 past studies that meet these criteria. These studies span temperatures of 800–2000 K, pressures of 0.1–8 bar, p_{O2} of 10^{-4}–0.5 bar, and p_{OH} of 10^{-6}–10^{-2} bar. Additional details on the data compilation are given below.

2.1. Premixed flames

Fenimore and Jones [20] reported three soot oxidation rates in premixed flames that were directly incorporated here. Neoh [9] reported 11 soot oxidation rates in premixed flames, which were based on surface area from light scattering. They reported that these surface areas were half of those determined from TEM, so their oxidation rates were multiplied by 0.5 before being incorporated here.

2.2. Diffusion flames

Lee et al. [24] reported 29 measurements in diffusion flames that were directly incorporated here.

Chan et al. [29] reported three measurements in a similar flame, for which their temperature overshoot corrections were used here. Both studies measured soot oxidation rates in soot columns confined by chimneys. This configuration yielded long soot oxidation regions of 6–9 cm. Neither study measured OH concentrations, which were assumed here to be negligible owing to the large distances above the stoichiometric regions. The optimizations presented below change only slightly upon the removal of the measurements of Refs. [24,29].

Garo et al. [13] reported six oxidation rate measurements, for which OH was measured with laser induced fluorescence (LIF) at a height of 50 mm and was estimated assuming partial equilibrium elsewhere. Owing to large uncertainties in the partial equilibrium assumption along diffusion flame centerlines [37], only the measurement at 50 mm is used here.

Kim and co-workers [8,11,12] did not report oxidation rates directly. These were found here from their measured OH concentrations and collision efficiencies, which were reported under the assumption of negligible oxidation by O_2.

Table 1
Summary of the 160 past measurements used here.

Study	Number of tests	Oxidant(s) measured
Premixed flames		
Fenimore and Jones [20]	3	O_2, OH
Neoh [9]	11	O_2, OH
Diffusion flames		
Chan et al. [29]	3	O_2
Garo et al. [13]	1	O_2, OH
Kim et al. [11]	12	O_2, OH
Kim et al. [12]	9	O_2, OH
Lee et al. [24]	29	O_2
Puri et al. [14,15]	5	O_2, OH
Xu et al. [8]	21	O_2, OH
TGAs and flow reactors		
Chan et al. [29]	9	O_2
Fenimore and Jones [20]	2	O_2
Higgins et al. [36]	25	O_2
Kalogirou and Samaras [30]	6	O_2
Sharma et al. [31]	24	O_2

Puri et al. [14,15] reported soot oxidation rates in terms of $\rho_s\, df_s/dt$, where ρ_s is soot density, f_s is soot volume fraction, and t is time. These rates were converted here to $\dot{w}_{ox}$ according to an approximation [38,39] that neglects gas density variations along the soot pathlines,

$$\dot{w}_{ox} = \frac{d_p}{6}\frac{\rho_s}{f_s}\frac{df_s}{dt}, \tag{5}$$

where d_p is soot primary particle diameter.

2.3. TGAs and flow reactors

The TGA and flow reactor studies of Table 1 are at relatively low temperatures with negligible hydrogen in any form. Therefore none of these studies measured OH concentrations, and it is assumed here that OH concentrations were negligible for these tests.

The nine TGA measurements of Chan et al. [29] and the two flow reactor measurements of Fenimore and Jones [20] were directly incorporated here. Higgins et al. [36] provided curve fits of $\dot{w}_{ox}$, which were used to obtain soot oxidation rates at the 25 locations in their flow reactor with reported temperatures.

In the TGA study of Kalogirou and Samaras [30], oxidation rates were expressed in terms of $m^{-1}\, dm/dt$, where m is the mass of soot in the TGA. These were converted here according to

$$\dot{w}_{ox} = (d_p\rho_s/6m)dm/dt, \tag{6}$$

and assuming ρ_s = 1850 kg/m^3 [8] and d_p = 40 nm [40]. Results from synthetic soot and from non-isothermal tests were excluded. Oxidation rates were found from their correlation at the six locations with reported temperatures.

Sharma et al. [31] measured oxidation rates of diesel soot in an isothermal TGA. Their mass conversion factors were used here to find oxidation rates from Eq. (6), again assuming ρ_s = 1850 kg/m^3 and d_p = 40 nm. Oxidation rates were found here at 10 min intervals, which was the longest time for which the rates were nearly constant.

3. Comparison of existing models with measurements

The 160 measurements of Table 1 allow a comprehensive evaluation of the predictions of the two leading soot oxidation models: Neoh and co-workers [9,10] for OH and NSC [21] for O_2. The resulting measured (meas) versus predicted (pred) soot oxidation rates are shown in Fig. 3. The measured oxidation rates span more than seven orders of magnitude. The coefficient of determination about the line of perfect agreement is R^2 = 0.79. The predicted rates are generally higher than the measured. More specifically, for the data of Fig. 3 the ratio $\dot{w}_{ox,pred}/\dot{w}_{ox,meas}$ has a geometric mean of 3.35. As will be shown below, the NSC O_2 model is primarily responsible for these overpredictions, with a slight contribution from the Neoh and co-workers [9,10] OH model.

4. Soot oxidation rate optimization

Following Glassman and Yetter [41], the OH and O_2 consumption rates were compared with OH and O_2 diffusion rates for the conditions of Table 1. Binary diffusivity between N_2 and the oxidizers was assumed. In all cases the diffusion of oxidizers to the soot surface was faster than their consumption there such that oxidation rates were not limited by gas phase diffusion [9,29]. This may not be the case for larger particles like coal or higher pressures like diesel engines [42] and shock tubes [23]. When gas phase diffusion is fast, the soot oxidation rate for constant collision efficiency and constant activation energy is:

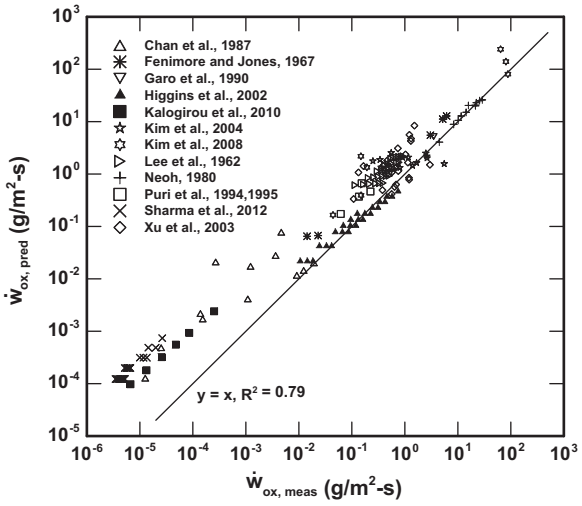

Fig. 3. Comparison of the measured and predicted soot oxidation rates using Neoh et al. [9] for OH and NSC [21] for O_2.

$$\dot{w}_{ox,i} = 0.25\eta_i[i]\,\bar{u}_i\,C_i\,\exp(-E_{A,i}/R_u\,T), \tag{7}$$

where i denotes the oxidizer (OH or O_2), brackets denote concentrations, $\bar{u}$ is mean molecular velocity, and C_i is the mass of carbon removed per reactive collision (12 and 24 g/mol for OH and O_2). It is commonly assumed [8–15] that $E_{A,OH}$ is negligible, as was confirmed here by correlations of the measurements of Table 1.

Assuming a Maxwell–Boltzmann distribution [39],

$$\bar{u}_i = (8R_uT/\pi MW_i)^{0.5}. \tag{8}$$

Combining Eqs. (7) and (8) yields soot oxidation rate expressions for OH and O_2:

$$\dot{w}_{ox,OH} = (1.27\times10^{-2}\ \mathrm{K^{0.5}\ s/m})\,\eta_{OH}\,p_{OH}\,T^{-0.5}, \quad \text{and} \tag{9}$$

$$\dot{w}_{ox,O2} = A_{O2}\,p_{O2}\,T^{-0.5}\,\exp(-E_{A,O2}/R_u\,T), \tag{10}$$

where A_{O2} is the pre-exponential factor.

Optimized values of η_{OH}, A_{O2}, and E_{O2} were found by maximizing the R^2 between the measured and predicted oxidation rates using MATLAB. The optimized soot oxidation rate expressions are:

$$\dot{w}_{ox,OH} = (1.27\times10^{-3}\,\mathrm{K^{0.5}\,s/m})p_{OH}T^{-0.5}, \ \text{i.e.,}\ \eta_{OH} = 0.10, \ \text{and} \tag{11}$$

$$\dot{w}_{ox,O_2} = (15.8\,\mathrm{K^{0.5}\,s/m})p_{O2}T^{-0.5}\exp\left(\frac{-195\,\mathrm{kJ/mol}}{R_uT}\right). \tag{12}$$

The resulting predictions are compared with the measured oxidation rates in Fig. 4. These have an R^2 about the line of perfect agreement of 0.98. This level of agreement indicates that the soot destruction for these conditions can be attributed to oxidation by OH and O_2, and that any variations arising from soot morphology are negligible. Fig. 4 corrects the large overpredictions of Fig. 3 primarily by reducing the O_2 predictions of NSC [21], and only slightly by reducing the OH predictions of Neoh and co-workers [9,10].

The error of each prediction is defined here as

$$E = \left|\dot{w}_{ox,pred}/\dot{w}_{ox,meas} - 1\right|. \tag{13}$$

The geometric mean of E for the data of Fig. 4 is 0.34. Thus, ±34% is a reasonable estimate of the errors to expect when Eqs. (11) and (12) are applied to similar soot oxidation processes.

The OH collision efficiency of Eq. (11) is in reasonable agreement with those of Neoh and co-workers [9,10], but others have proposed collision efficiencies in the range of 0.01–0.4 [8,11–15]. The activation energy of Eq. (12) is higher than previously reported [3–6,27,29–31]. The prediction of Eq. (12) for flame 1 of Xu et al. [8] is shown in Fig. 2, and for these conditions it is generally between the predictions of Refs. [21,24].

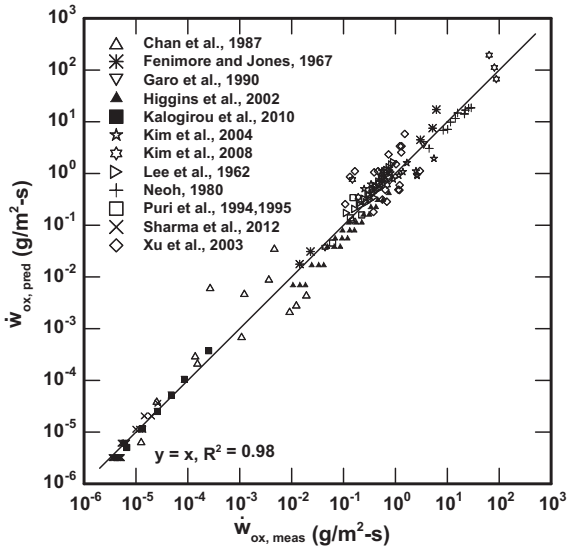

Fig. 4. Comparison of the measured and predicted soot oxidation rates using the rate expressions of Eqs. (11) and (12).

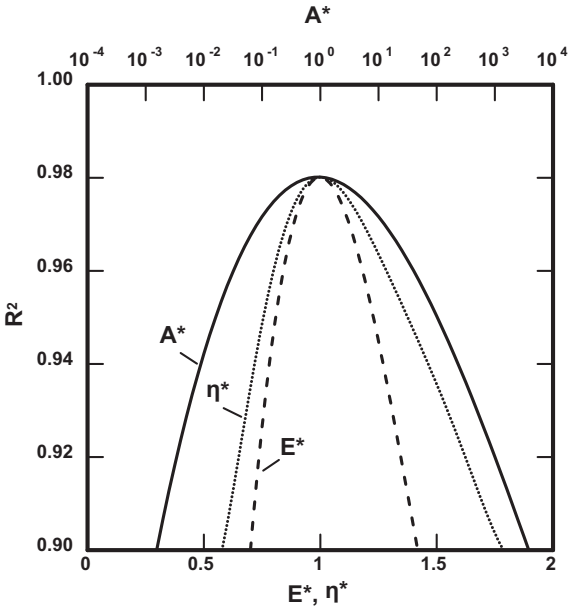

Fig. 5. Sensitivity of the maximized obtainable R^2 when one of η_{OH}, $E_{A,O2}$, or A_{O2} is displaced from its optimized value.

Several studies have identified OH as the dominant soot oxidant in flames [8,9,11,12]. Equations (11) and (12) allow the relative importance of OH and O_2 to be quantified for the 62 flame conditions in Table 1 with measured OH concentrations, namely the premixed and diffusion flame studies of Refs. [8,9,11–15,20]. For each condition, the ratio of predicted OH and O_2 oxidation rates, $\dot{w}_{ox,OH}/\dot{w}_{ox,O2}$, was found from Eqs. (11) and (12). This ratio had an approximately lognormal distribution with a geometric mean of 4.7 and a geometric standard deviation of 3.6. In premixed flames OH nearly always dominates, owing to radical overshoot [37]. Although OH also dominates in most diffusion flames, O_2 domination occasionally occurs in diffusion flames.

In plots like that of Fig. 4, the sensitivity of R^2 to η_{OH}, $E_{A,O2}$, and A_{O2} was examined, with results summarized in Fig. 5. Here each

parameter is normalized by its optimized value, i.e., $\eta^*_{OH} = \eta_{OH}/0.10$; $E^* = E_{A,O2}/(195\ kJ/mol)$; and $A^* = A_{O2}/(15.8\ K^{0.5}\ s/m)$. Displacements above about ±30% in η_{OH} or $E_{A,O2}$ from their optimized values cannot be compensated for by adjustments to the other two parameters and the predictions deteriorate. This indicates there is an uncertainty of about ±30% in the optimized η_{OH} and $E_{A,O2}$.

The greatest uncertainty in this work arises from the measurements of OH concentrations, for which estimated uncertainties are on the order of ±30% [8,11,12]. Partial equilibrium estimates of OH concentrations have comparable uncertainties. However, modern CFD codes that match other measurements in flames may be able to predict OH concentrations with less uncertainty.

5. Conclusions

Past experimental work was examined to identify measurements that could lead to improved models of soot oxidation by OH and O_2. Twelve suitable studies were identified. These contained 160 measurements at temperatures of 800–2000 K, pressures of 0.1–8 bar, OH partial pressures of 10^{-6}–10^{-2} bar, O_2 partial pressures of 10^{-4}–0.5 bar, and oxidation rates of 10^{-6}–100 g/m^2 s. The measurements were correlated to yield new rate models of soot oxidation by OH and O_2. The key findings are:

1. Soot oxidation by OH has a negligible activation energy. The rate of soot oxidation by OH is best correlated by Eq. (11). In other words, soot oxidation by OH has a collision efficiency of 0.10, which is in reasonable agreement with several past models.
2. The NSC [21] model overpredicts rates of soot oxidation by O_2. The rate of soot oxidation by O_2 is best correlated by Eq. (12). The associated activation energy is 195 kJ/mole, which is higher than that of any previous model.
3. When combined, the new soot oxidation models for OH and O_2 yield soot oxidation rates in agreement with the measurements with an R^2 of 0.98. For this data the new models match the measured soot oxidation rates with a mean error of ±34%.
4. For premixed and diffusion flames, the optimized models indicate that soot oxidation by OH dominates over that by O_2.

Acknowledgment

This work was supported by the National Science Foundation (NSF) Grant No. CBET0954441.

References

[1] Stanmore BR, Brilhac JF, Gilot P. The oxidation of soot: a review of experiments, mechanisms and models. Carbon 2001;39:2247–68.
[2] Howard JB. Carbon addition and oxidation reactions in heterogeneous combustion and soot formation. Proc Combust Inst 1990;23:1107–27.
[3] Smith IW. The combustion rates of coal chars: a review. Proc Combust Inst 1982;19:1045–65.
[4] Frenklach M, Wang H. Detailed modeling of soot particle nucleation and growth. Proc Combust Inst 1990;23:1559–66.
[5] Kazakov A, Wang H, Frenklach M. Detailed modeling of soot formation in laminar premixed ethylene flames at a pressure of 10 bar. Combust Flame 1995;100:111–20.
[6] Appel J, Bockhorn H, Frenklach M. Kinetic modeling of soot formation with detailed chemistry and physics: laminar premixed flames of C2 hydrocarbons. Combust Flame 2000;121:122–36.
[7] Wright FJ. The oxidation of soot by O atoms. Proc Combust Inst 1975;15:1449–60.
[8] Xu F, El-Leathy AM, Kim CH, Faeth GM. Soot surface oxidation in hydrocarbon/air diffusion flames at atmospheric pressure. Combust Flame 2003;132:43–57.
[9] Neoh KG. Soot burnout in flames. Cambridge (MA): MIT; 1980 [dissertation].
[10] Neoh KG, Howard JB, Sarofim AF. Effect of oxidation on the physical structure of soot. Proc Combust Inst 1984;20:951–7.
[11] Kim CH, El-Leathy AM, Xu F, Faeth GM. Soot surface growth and oxidation in laminar diffusion flames at pressures of 0.1–1.0 atm. Combust Flame 2004;136:191–207.
[12] Kim CH, Xu F, Faeth GM. Soot surface growth and oxidation at pressures up to 8.0 atm in laminar nonpremixed and partially premixed flames. Combust Flame 2008;152:301–16.
[13] Garo A, Prado G, Lahaye J. Chemical aspects of soot particles oxidation in a laminar methane-air diffusion flame. Combust Flame 1990;79:226–33.
[14] Puri R, Santoro RJ, Smyth KC. The oxidation of soot and carbon monoxide in hydrocarbon diffusion flames. Combust Flame 1994;97:125–44.
[15] Puri R, Santoro RJ, Smyth KC. Erratum. Combust Flame 1995;102:226–8.
[16] Mehta RS, Haworth DC, Modest MF. An assessment of gas-phase reaction mechanisms and soot models for laminar atmospheric-pressure ethylene–air flames. Proc Combust Inst 2009;32:1327–34.
[17] Leung KM, Lindstedt RP, Jones WP. A simplified reaction mechanism for soot formation in nonpremixed flames. Combust Flame 1991;87:289–305.
[18] Liu F, Guo H, Smallwood GJ, Gulder OL. Numerical modelling of soot formation and oxidation in laminar coflow non-smoking and smoking ethylene diffusion flames. Combust Theor Model 2003;7:301–15.
[19] Connelly BC, Long MB, Smooke MD, Hall RJ, Colket MB. Computational and experimental investigation of the interaction of soot and NO in coflow diffusion flames. Proc Combust Inst 2009;32:777–84.
[20] Fenimore CP, Jones GW. Oxidation of soot by hydroxyl radicals. J Phys Chem 1967;71:593–7.
[21] Nagle J, Strickland-Constable RF. Oxidation of carbon between 1000 °C and 2000 °C. Proceedings of the 5th conference on carbon. Pergamon Press; 1962.
[22] Smooke MD, McEnally CS, Pfefferle LD, Hall RJ, Colket MB. Computational and experimental study of soot formation in a coflow, laminar diffusion flame. Combust Flame 1999;117:117–39.
[23] Park C, Appleton JP. Shock-tube measurements of soot oxidation rates. Combust Flame 1973;20:369–79.
[24] Lee KB, Thring MW, Beer JM. On the rate of combustion of soot in a laminar soot flame. Combust Flame 1962;6:137–45.
[25] Slavinskaya NA, Frank P. A modelling study of aromatic soot precursors formation in laminar methane and ethene flames. Combust Flame 2009;156:1705–22.
[26] Blanquart G, Pitsch H. Analyzing the effects of temperature on soot formation with a joint volume-surface-hydrogen model. Combust Flame 2009;156:1614–26.
[27] Bisetti F, Blanquart G, Mueller ME, Pitsch H. On the formation and early evolution of soot in turbulent nonpremixed flames. Combust Flame 2012;159:317–35.
[28] Lin CY, Lin MC. Kinetics of the $C_6H_5 + O_2$ reaction. In: Eastern states section of the combustion institute fall technical meeting, Nov 2–5, Gaithersburg, MD, USA; 1987.
[29] Chan ML, Moody KN, Mullins JR, Williams A. Low-temperature oxidation of soot. Fuel 1987;66:1694–8.
[30] Kalogirou M, Samaras Z. Soot oxidation kinetics from TG experiments. J Therm Anal Calorim 2010;99:1005–10.
[31] Sharma HN, Pahalagedara L, Joshi A, Suib SL, Mhadeshwar AB. Experimental study of carbon black and diesel engine soot oxidation kinetics using thermogravimetric analysis. Energ Fuel 2012;26:5613–25.
[32] Jaramillo IC, Gaddam CK, VanderWal RL, Huang CH, Levinthal JD, Lighty JS. Soot oxidation kinetics under pressurized conditions. Combust Flame 2014;161:2951–65.
[33] Zhang Y, Boehman AL. Oxidation behavior of soot generated from the combustion of methyl 2-butenoate in a co-flow diffusion flame. Combust Flame 2013;160:112–9.
[34] Raj A, Yang SY, Cha D, Tayouo R, Chung SH. Structural effects on the oxidation of soot particles by O_2: experimental and theoretical study. Combust Flame 2013;160:1812–26.
[35] Raj A, Tayouo R, Cha D, Li L, Ismail MA, Chung SH. Thermal fragmentation and deactivation of combustion-generated soot particles. Combust Flame 2014;161:2446–57.
[36] Higgins KJ, Jung H, Kittelson DB, Roberts JT, Zachariah MR. Size-selected nanoparticle chemistry kinetics of soot oxidation. J Phys Chem A 2002;106:96–103.
[37] Mitchell RE, Sarofim AF, Clomburg LA. Partial equilibrium in the reaction zone of methane-air diffusion flames. Combust Flame 1980;37:201–6.
[38] Sunderland PB, Koylu UO, Faeth GM. Soot formation in weakly buoyant acetylene-fueled laminar jet diffusion flames burning in air. Combust Flame 1995;100:310–22.
[39] Sunderland PB, Faeth GM. Soot formation in hydrocarbon/air laminar jet diffusion flames. Combust Flame 1996;105:132–46.
[40] Clague ADH, Donnet JB, Wang TK, Peng JCM. A comparison of diesel engine soot with carbon black. Carbon 1999;37:1553–65.
[41] Glassman I, Yetter RA. Combustion. 4th ed. Academic Press; 2008. p. 528.
[42] Song J, Song C, Lv G, Wang L, Bin F. Modification to Nagle/Strickland-Constable model with consideration of soot nanostructure effects. Combust Theor Model 2012;16:639–49.